Rock mechanical modelling of the Bentonite Rock Interaction Experiment, Äspö Hard Rock Laboratory, Sweden

Åsa Fransson[a,*], Margareta Lönnqvist[b], Giulio Viola[c]

[a] *University of Gothenburg, Department of Earth Sciences, SE-405 30 Gothenburg, Sweden*
[b] *Clay Technology AB, IDEON Science Park, SE-223 70 Lund, Sweden*
[c] *University of Bologna, Department of Biological, Geological, and Environmental Sciences, Via Zamboni 67, 40126 Bologna, Italy*

A B S T R A C T

The Bentonite Rock Interaction Experiment (BRIE) was performed in a tunnel at a depth of 420 m at the Äspö Hard Rock Laboratory in Sweden. The experiment focused on the hydraulic properties of rock and bentonite aiming at investigating the exchange of water across a bentonite-rock interface. The hypothesis for the mechanical modelling presented here was that changes in flow (observed in rock and on bentonite parcels) were due to local mechanical deformation. Induced stresses related to the construction (and experimental) stages for the BRIE site such as excavation of tunnels, drilling and over-coring of two vertical, tunnel-floor boreholes and, finally, installation and swelling of bentonite, were expected to be the main causes of these deformations. We assumed that this could be investigated using a step-wise rock mechanical modelling approach (with a relevant modelling sequence) and validated by using a transdisciplinary approach including field structural geological mapping (geometric, kinematic and dynamic interpretation of the exposed fracture sets) and hydrogeological investigations.

For key fractures intersecting the boreholes, the modelled fracture normal and shear displacements were found to be local, small, and in line with field observations and measurements for BRIE. Results point at an agreement between the spatial locations of changes in flow identified from the bentonite parcels and the locations of inelastic deformation indicated by mechanical modelling for a reverse stress regime. Besides providing information about the key fractures, the structural mapping allowed to establish solid relationships between brittle structural features in the tunnel and in the cores, which were used as, or compared to, the main fracture input to the rock mechanical modelling. The identified fracture sets were found to be structurally reconcilable with the larger-scale tectonic picture of the area.

1. Introduction

An important task for a society that aims at sustainability is to be able to conceptualise, characterise and model different geological systems. The ability to transmit and store fluids and energy, the chemistry of transmitted fluids as well as the rock mechanical behaviour all relate to the properties of the geological system. Descriptions may focus on one or several of the aspects above, but key is to have focus on the purpose or purposes identified by the specific investigation and modelling task. A model has to capture key processes (e.g. hydraulics, mechanics) and related features and material properties to deliver a relevant and meaningful representation of the system at hand.

The Bentonite Rock Interaction Experiment (BRIE)[1], which had its focus on the hydraulic properties of rock and bentonite and that investigated the exchange of water across a bentonite-rock interface, was

performed at the Äspö Hard Rock Laboratory (Äspö HRL) in Sweden between 2010 and 2014. The experiment was conceived in the framework of the research efforts for a future underground nuclear waste repository. The multibarrier Swedish concept for nuclear waste underground storage includes a natural barrier (the crystalline rock) and two engineered barriers, bentonite and a copper canister.[2]

BRIE included three characterisation phases: selection of site (by investigating the tunnel and logging five vertical boreholes); characterisation of site (analysis of the tunnel and 18 additional boreholes, both horizontal and vertical) and; characterisation of two 300 mm boreholes (vertical and referred to as 17G01 and 18G01). This was followed by installation of bentonite parcels in boreholes 17G01 and 18G01 as well as monitoring of sensors and final extraction and analysis of bentonite parcels and of the surrounding rock. The main objectives of BRIE and the related modelling task[3–6] were to increase the scientific

understanding of the exchange of water across the interface, to provide better predictions (models) of the wetting of bentonite and to identify better characterisation methods of the deposition holes (geology and hydrogeology).

The hypothesis stated for the mechanical modelling presented in this paper was that changes in flow (observed in rock and on bentonite) for BRIE were due to local mechanical deformation. We assumed that this could be investigated using step-wise rock mechanical modelling (with a relevant modelling sequence) and validated using structural geological mapping (geometric, kinematic and dynamic interpretation of the exposed fracture sets) and performed hydrogeological investigations.

The rock mechanical modelling was used to investigate potential normal- and shear displacements induced by the tunnel construction and the experimental stages related to BRIE. Displacement was investigated at selected points along key fractures and compared to hydrogeological observations in the rock and on the bentonite parcels. In addition, the magnitudes of the tangential stresses around the vertical 300 mm boreholes in the tunnel floor were studied. We assumed that the detected increase in water flow occurred as a consequence of mechanical deformation due to changes in the boundary geometrical conditions and induced stresses. We expected a clear hydromechanical response in space and through time for relevant in situ stress conditions. Structural mapping was used to increase the chance of identifying larger fractures (by mapping, e.g., displacement). Kinematic indicators (e.g. slickensided surfaces) were used to constrain fault and fracture kinematics. Structural geological properties favourable to deformation would add to the likelihood of mechanical deformation. This work is important since it exemplifies how transdisciplinary investigations, basic system descriptions and knowledge exchange related to geomechanics, hydrogeology and structural geology, can give additional (independent) constraints to parameters and system behaviour.

2. Geological setting

Äspö HRL is situated in southeast Sweden, see Fig. 1a and in the southwestern part of the Fennoscandian shield.[7] In general, the composition of the main rock types is quartz monzodioritic and granodioritic. In addition, dikes, veins and minor bodies of fine-grained granite, pegmatite and composite intrusions can be found.

The BRIE site (Fig. 1a, indicated by a small red circle) is located in a tunnel at approximately − 420 m. Fig. 1b shows the experimental site (the tunnel TASO), four horizontal boreholes in the tunnel wall and an area (A). Fig. 1c includes all 19 tunnel floor boreholes within the area (A). The boreholes investigated have shown gabbroid-dioritoid and fine grained granite as main rock types. In addition rock occurrences (veins and dykes) with pegmatite and fine grained granite were identified, see example of rock core from hole 18G01 in Fig. 2.
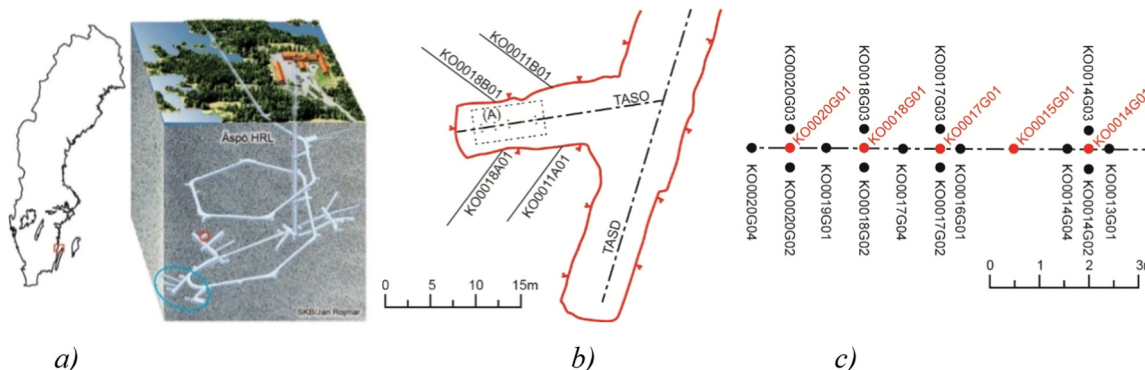

Fig. 2. Rock cores and bentonite (including vertical wetted trace, dashed line). Comparison of some fractures in rock core and traces (white lines) on bentonite for hole 18G01[1].

Geological and hydrogeological investigations for BRIE resulted in a geometric framework that included the main water-bearing features identified in the tunnel and in the lower sections of boreholes 17G01 and 18G01. Main features were two deformation zones intersecting the full perimeter of the tunnel and water-bearing structures intersecting the two 300 mm boreholes.

3. Methodology

The rock mechanical modelling presented in this paper included a modelling sequence representing construction and experimental stages for the site and for BRIE: 1) Initial undisturbed conditions at the site; 2) Excavation of tunnels TASO and TASD, see Fig. 1b; 3) Pressurisation of fractures; 4) Excavation of 300 mm holes through over-coring of 76-mm boreholes KO0017G01 and KO0018G01, see Fig. 1c; 5) Application of swelling pressure in the 300 mm holes as a consequence of the installation of bentonite parcels.

Modelling steps 1–3 above aimed at representing initial conditions i.e. stepwise modelling of the past construction of the experimental site (TASO) that was used for BRIE and steps 4 and 5 represent the experiment itself. All steps in this modelling sequence will be used to

Fig. 1. a) Äspö Hard Rock Laboratory (Äspö HRL), b) the site for BRIE (the TASO-tunnel and the horizontal boreholes) and c) vertical tunnel floor boreholes within the area (A), see illustration b).
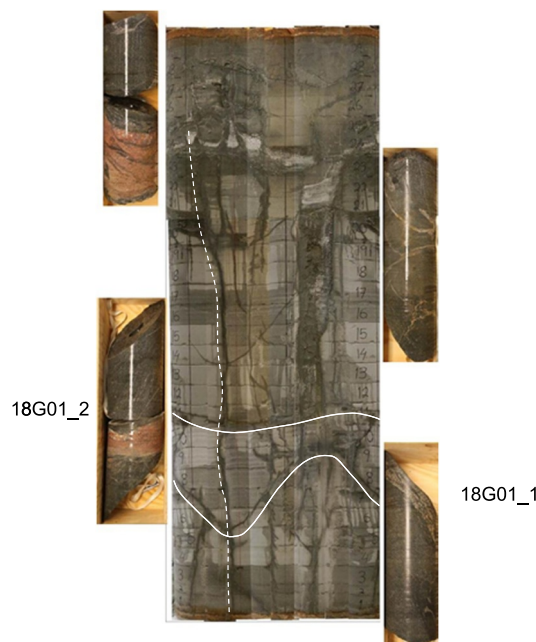
present the results from rock mechanical modelling, see e.g. steps 1–5c on the horizontal axis in Fig. 10, representing specific points on selected fractures, referred to as history points, see Fig. 9.

The initial characterisation of the site[1] (between steps 3 and 4 in the modelling sequence above) aimed at investigating if TASO was a suitable site for BRIE. This included five 3 m long and 76 mm in diameter vertical boreholes that were core-drilled along the centre line of the TASO tunnel (Fig. 1b and c). Boreholes were named KO0014G01, KO0015G01, KO0017G01, KO0018G01 and KO0020G01 according to a system used at Äspö HRL (Fig. 1c; in the text referred to in here as 17G01, 18G01 etc). A more detailed characterisation of the site followed based on 14 additional vertical boreholes of 76 mm in diameter (Fig. 1c). Most of these were drilled to a depth of 3.0–3.5 m from the tunnel floor, whereas the four holes surrounding 14G01 had a depth of 1.5 m, due to a deformation zone identified in the proximity of the boreholes and the wish to maintain good quality rock. In addition, four horizontal 10 m long and 76 mm in diameter cored boreholes were drilled into the two tunnel walls to further investigate the rock and allow follow up studies of the hydraulic head (Fig. 1b).

For step 4 of the modelling sequence, the two floor central boreholes, 17G01 and 18G01, were over-cored, leading to two 300 mm boreholes. These were also investigated using geological mapping and hydraulic testing.[1] The 5th, final, step of the modelling sequence included the application of a swelling pressure in the 300 mm holes due to swelling of bentonite.

Three key issues were addressed by the modelling. The first issue was how different types of in situ stress regimes (strike slip- or reverse type stress fields) influence the response of the fractures to changes in load using the modelling sequence (1 − 5). For this, four different in-situ stress models were considered (two were strike-slip type and two were reverse type stress regimes).

The second issue was the potential interaction between two fractures, 18G01_1 and 18G01_2, in the lower part of 18G01, see Fig. 2 (i.e., if shearing in combination with normal deformation of one fracture causes dilation of the other fracture). Finally, third issue, we investigated if the stresses in the most stress-relaxed parts of the rock around 18G01 would be sufficiently low, after excavation of the 300 mm hole or after a swelling pressure of the bentonite has developed, to create a vertical structure such as the one observed as a wetted trace in the bentonite (dashed line), cf. Fig. 2.

In this paper, all BRIE construction- and experimental stages and the rock mechanical modelling were used to provide information on the natural and induced rock stress and the brittle deformation history of the chosen site. The data were integrated and semi-quantitatively studied against the detailed structural mapping of the tunnel and cores and the hydrogeological observations and measurements at the site, see Field observations and measurements in Section 5.4.

4. Description of numerical models

4.1. Model types

Three types of models were considered. These included a large-scale model of TASO and its access tunnel TASD (model type 1, see Fig. 4a). This type of model was primarily used to derive boundary conditions for the smaller and more detailed near-field models. The second model was a near-field model with 300 mm holes and fractures (model type 2, Fig. 4b). This type of model was used to address the first and second issues, impact of in situ stress regime and interaction between two fractures in 18G01 (18G01_1 and 18G01_2), see Fig. 2 Finally, a linear elastic near-field model of the rock surrounding 18G01 (model type 3, Fig. 4c) was used to address the third and final issue related to tangential stresses at the orientation corresponding to the wetted trace on the bentonite (dashed line), Fig. 2.

4.2. Modelling tool

The numerical modelling was conducted using the distinct element code *3DEC, v. 5.00*.[8] *3DEC* was developed for analyses of mechanical processes in discontinuous materials such as fractured rock and has been used extensively to address different types of rock mechanics issues related to nuclear waste disposal in crystalline rock. *3DEC* models are constructed from an assemblage of blocks where the interfaces between the blocks represent fractures. The blocks are divided into a mesh of tetrahedral finite-difference elements where each element responds to a prescribed stress-strain law. It was assumed in all models presented in this paper that the blocks (simulating the intact rock between and surrounding the fractures) respond to loading as an isotropic and linear elastic material. In models without explicitly represented fractures (such as model types 1 and 3), all interfaces between the blocks were "glued together" to simulate a homogeneous and continuous linear elastic rock mass. These models were analysed using the default "large strain" option.

In models with fractures (model types 1 and 2), the relative movements of the fracture surfaces were assumed to be governed by an idealized elastic-plastic constitutive relation with Mohr-Coulomb strength. These models were analysed using the "small strain" option in *3DEC*[8,9] to avoid numerical disturbances that may otherwise occur along block boundaries when fracture shear displacements become large.[10]

4.3. Model geometry

4.3.1. Large-scale models

The large-scale models consisted of a cube with side-length 60 m in which the TASO tunnel and its access tunnel TASD were included. All tunnels have a small inclination and were, therefore, approximated to be horizontal. Two fracture zones intersect the full perimeter of the outer parts of TASO (see Fig. 3). Red arrows mark the distances from the inner end of the TASO-tunnel to the points where the fracture zones included in the models intersect the centre line of the roof (1.8 m for ID 04 - strike/dip 128/70 and 5.4 m for ID 10 & 12 - strike/dip 318/75, being the average orientation of fractures 10 & 12). Strike transformed from magnetic north to RT90. Presence of damage zone and core as well
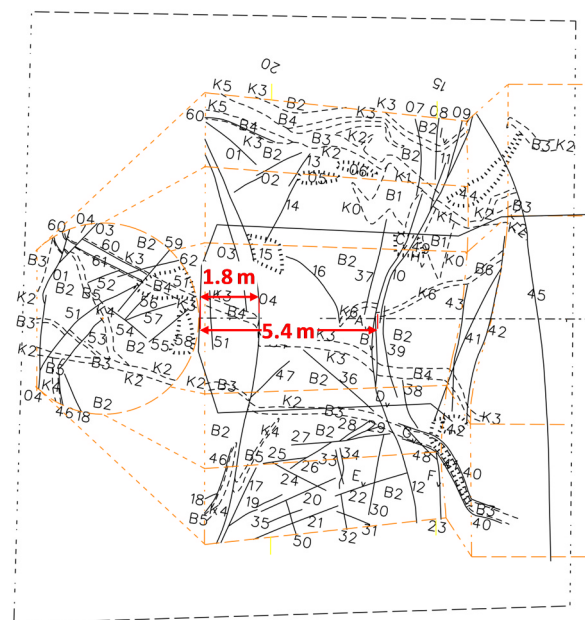

Fig. 3. Tunnel mapping. Fracture mapping of TASO. Two fracture zones intersect the full perimeter of the outer parts of TASO (ID 04 at 1.8 m and ID 10 & 12 at 5.4 m).
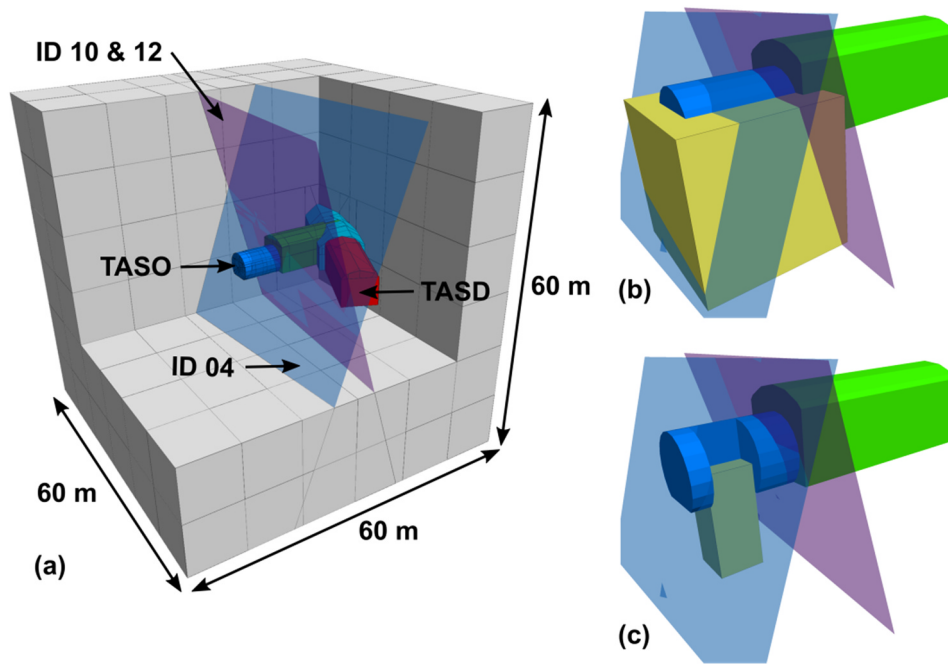
Fig. 4. Model geometry. a) Geometry of large-scale models (type 1). b) Location of model type 2 (yellow cube) in relation to TASO. c) Location of model type 3 (grey-green rectangular block).

as finite displacement were key aspects when identifying or confirming these features using structural geological mapping, see Section 5.4.1

These two features were included in the models and extended to the boundaries of it. An illustration of the model is provided in Fig. 4a. The locations of the near-field models in relation to the large-scale model are indicated in Fig. 4b and Fig. 4c, respectively. Note that parts of the model or tunnel are hidden to expose the tunnels, fracture zones or near-field model volume.

4.3.2. Near-field models with fractures

The near-field models with fractures consisted of a cube with side-length 10 m in which the two 300 mm holes (17G01 and 18G01) were explicitly represented. The borehole lengths are 3.5 m (17G01) and

3.1 m (18G01), respectively. Four smaller fractures intersecting 17G01 and 18G01 were included in the model (Fig. 5, fracture IDs used in this study are given in brackets). The four fractures are a fracture identified on the core and in the bentonite parcel in hole 17G01 (17G01_1); and a vein that terminates against 17G01_1 (17G01_2). Further, Fig. 2 shows the fracture identified on the core and in the bentonite parcel in 18G01 (18G01_1); and the sub-horizontal fracture found above 18G01_1 (18G01_2). These fractures were also identified being representatives of the main fracture sets, see Field observations and measurements in Section 5.4.

All fractures were implemented in the model as planar circular features with a radius set at 1.0 m. The centre of each fracture was located on the respective borehole axis. Orientations and depths in the
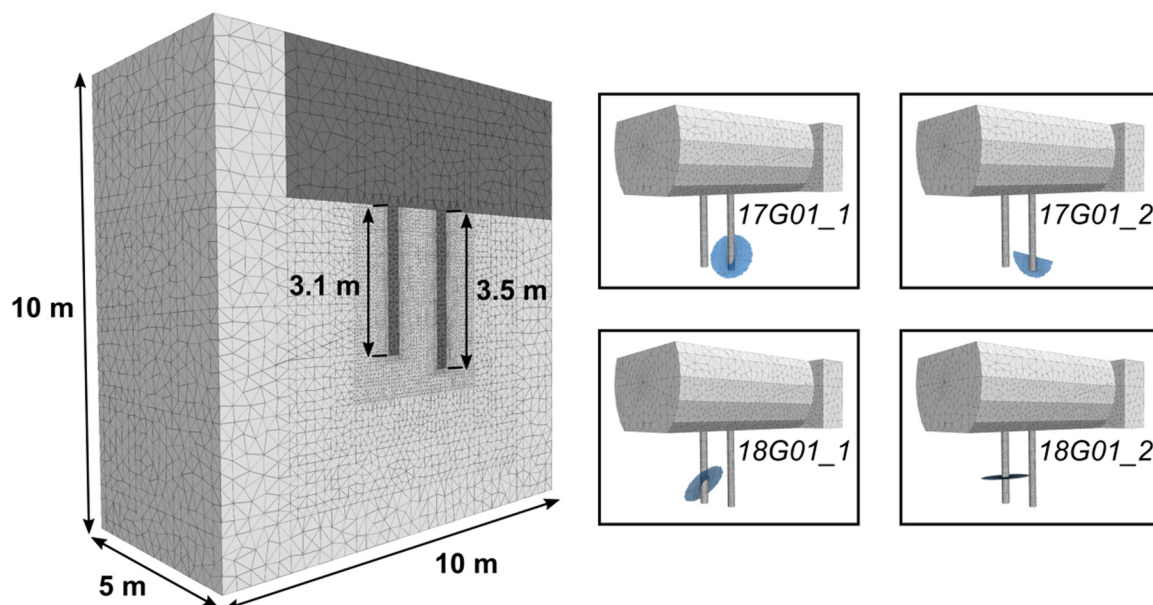

Fig. 5. Near-field model. a) Geometry of the near-field models with fractures (type 2, see Fig. 4b) including 300 mm holes (18G01, left and 17G01, right). b) Locations of key fractures (in blue) with respect to the tunnel and 300 mm holes.

Table 1
Fracture model. Strike in RT90.

Fracture ID	Orientation (strike,°/dip,°)	Depth in borehole (m)	Radius (m)
17G01_1	106/66	2.86	1.0
17G01_2	291/85	2.86	1.0
18G01_1	212/53	2.30	1.0
18G01_2	222/4	1.99	1.0

boreholes are presented in Table 1. Note that parts of the model are hidden to expose the tunnel and the 300 mm hole, see Fig. 5. Darker shaded regions represent interior of the tunnel, 17G01 and 18G01.

Although the fracture zones intersected the near-field model volume (see Fig. 4b), these large structures were not explicitly included in the model: (1) A disturbance of the stress-field at the locations of the 300 mm holes and fractures due to the fractures zones was accounted for by means of the boundary conditions extracted from the large-scale models (cf. Section 4.7). (2) Stress redistribution effects around excavations are only noticeable a few diameters away from the openings.[11] Given the dimensions and locations of 17G01 and 18G01, stress redistribution effects around these holes will influence the stability of the small fractures but not the fracture zones.

4.3.3. Linear elastic models

The linear elastic near-field models consisted of a rectangular block with side-lengths 3 m (along tunnel), 3 m (across tunnel) and 6.85 m (vertically) in which one 300 mm hole (18G01) was explicitly represented, see Fig. 6. Note that parts of the model are hidden to expose the 300 mm hole (18G01). Darker shaded regions represent interior of the tunnel and 18G01.

The borehole length was 3.1 m. Neither fracture zone intersected the near-field model volume (see Fig. 4c). However, any mechanical influence of these structures were accounted for by means of boundary conditions extracted from the large-scale models (cf. Section 4.7).

4.4. Material properties: rock, fractures and fracture zones

The rock was assumed to respond to load changes as a linear elastic material. The parameter values were set in accordance with those determined in the Äspö Pillar Stability Experiment, APSE[12] with a Young's
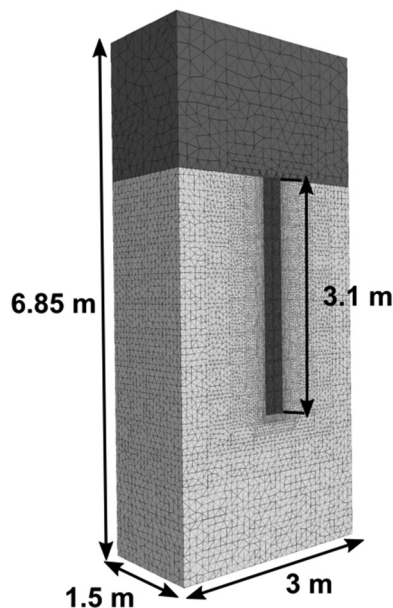

Fig. 6. Geometry of the linear elastic models, focus on hole 18G01 (type 3, see Fig. 4c).

Table 2
Material properties for the fractures and deformation zones (based on data from the Laxemar site investigation[13]). A lower alternative for the normal stiffness (in brackets) was assigned to 18G01_2 in some models.

Parameter	Unit	Discrete fractures	Fracture zones
Normal stiffness	GPa/m	700 (70)	700
Shear stiffness	GPa/m	40	40
Dilatancy angle	deg.	0	0
Friction angle	deg.	35	35
Cohesion	MPa	0	0

modulus of 76 GPa, a Poisson´s ratio of 0.25 and a tensile strength of 14.3 MPa. Note that the tensile strength is not an input parameter to any of the models. It was used in the post-processing of results from the linear elastic near-field models (type 3) to assess the potential for vertical tensile fractures to develop in the walls of the 300 mm holes.

For the fractures and fracture zones, an elastic/plastic material model with a Mohr-Coulomb shear strength criterion was chosen. The base-case property values were the same as those used in the modelling of the Prototype Repository experiment,[10] see Table 2. These, in turn, were based on data from the Laxemar site investigation.[13] To avoid non-physical movements caused by numerical disturbances an algorithm[14] was developed to ramp down the shear strength (cohesion) of a fracture at the beginning of each modelling step. In this study, the algorithm had been modified such that both the cohesion and the tensile strength were ramped down simultaneously at the beginning of each modelling step.

4.5. In situ stress models

The stress models considered in this study were based on stress measurements conducted in the TASK tunnel at Äspö HRL[15,16]: σ_H = 16–26 MPa (trend 140–155° RT90), σ_h = 9–14 MPa and σ_v = 10.5–18.1 MPa. From these measurements, four in situ stress models were constructed for use in the *3DEC* models (see Table 3). Models *a* and *b* were based on the maximum value of σ_H and are strike-slip type and reverse type stress regimes, respectively. Models *c* and *d* were based on the minimum value of σ_H and are strike-slip type and reverse type stress regimes, respectively. According to the stress measurements, the trend of σ_H deviates from the TASO tunnel axis by 68–83°. For the sake of simplicity and for the purpose of determining if a vertical tensile fracture with strike perpendicular to the tunnel axis can develop, it was assumed that the trend of σ_H is perpendicular to the tunnel axis in all stress models. Fig. 7 shows Mohr circle plots of the in situ state of stress, for each stress model, and stability margins of the selected fractures (coloured markers) and fracture zones (black markers). The pore pressure was 4 MPa. Further, the same legend applies to all sub-figures. With the exception of stress model *a* where fractures 17G01_1 and 17G01_2 are unstable initially, all fractures and fracture zones are stable initially.

Note that, in *3DEC*, compressive rock stresses are negative. For fracture normal stresses, the sign convention is reversed.

4.6. Pore pressure and internal pressure

All models follow a similar modelling sequence: (1) establishment of

Table 3
In situ stress models.

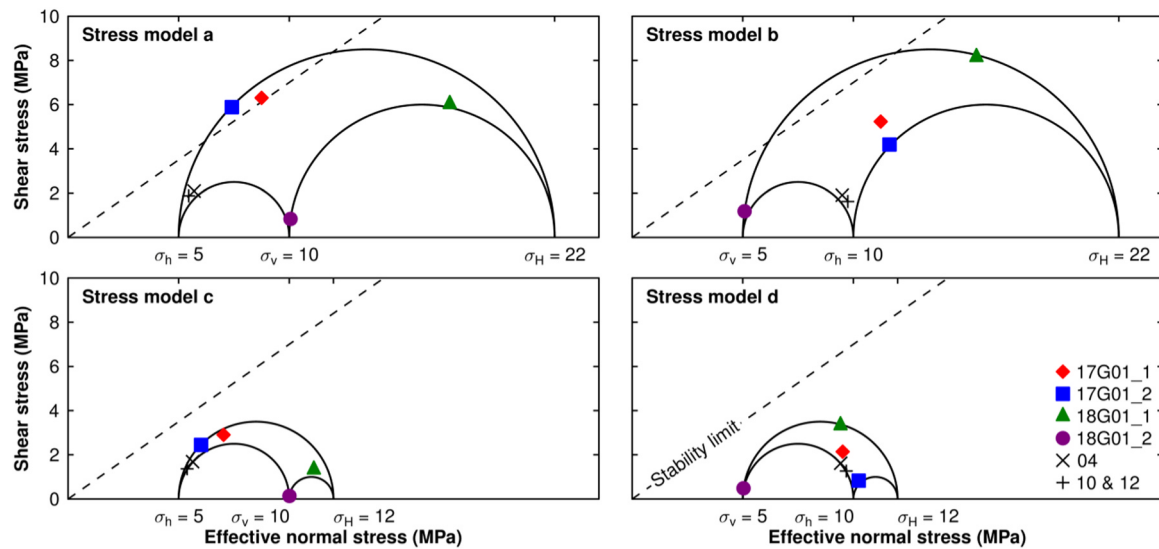| Stress component	Unit	Model a Strike-slip	Model b Reverse	Model c Strike-slip	Model d Reverse
σ_H	MPa	− 26	− 26	− 16	− 16
σ_h	MPa	− 9	− 14	− 9	− 14
σ_v	MPa	− 14	− 9	− 14	− 9

Fig. 7. Stability, selected fractures. Mohr circle plots of the in situ state of stress, for each stress model (cf. Table 3), and stability margins of the selected fractures and fracture zones.

a primary equilibrium (corresponding to initial undisturbed conditions at the site with hydrostatic groundwater pressure in the fractures and fracture zones) and (2) excavation of the tunnels with a small, generically chosen, drawdown of groundwater pressures. The modelling sequence for the smaller near-field models also includes the following steps: (3) a further, generically chosen, drawdown of the groundwater pressure followed by changes in water pressure (relative increase/decrease of 0–1 MPa set in agreement with hydraulic testing in TASO,[16] only model type 2; denoted pressurisation of the fractures), (4) excavation of the 300 mm holes and (5) application of a swelling pressure within the 300 mm holes.

The pore pressure was applied uniformly within the fracture zones and discrete fractures without regard of any spatial variations due to e.g., proximity to tunnels and holes. A summary of the input data is provided in Table 4. The swelling pressure was assumed to be the same in both 300 mm holes. It was applied as an internal hydrostatic boundary condition and was ramped up to the maximum value of 3 MPa in steps of 1 MPa (see Table 4).

4.7. Boundary conditions

For the large-scale models (type 1), the same boundary conditions were applied regardless of in situ stress model. The vertical boundaries were locked in the horizontal directions whereas the top and bottom boundaries were locked in all directions. It could be noted that this is not strictly necessary since the stress components are aligned with the model axes. The boundary conditions for the smaller near-field models (types 2 and 3) were extracted from corresponding large-scale models (i.e. with the same in situ stress model) and implemented in the models using the developed algorithm.[10] The near-field models were judged to be sufficiently large that the state of stress at the boundaries was not

affected by the excavation of the 300 mm holes.

4.8. Descriptions of analysed models

The models, analysed as part of this study, are compiled and listed below; the model's suffix (*a*, *b*, *c* or *d*) refers to the in situ stress model, cf. Table 3. The three main models in terms of geometry are presented in Fig. 4: Large-scale models (model type 1); Near-field models with fractures (model type 2); and; Linear elastic near-field models (model type 3).

The large-scale models (model type 1, Fig. 4a) include models with active fracture zones; one model for each in situ stress model (models 1a, 1b, 1c, 1d) and equivalent linear elastic models with identical geometry (models 1aE, 1bE, 1cE, 1dE). The near-field models with fractures (model type 2, Fig. 4b and Fig. 5) present models with base-case material properties (models 2a, 2b) and equivalent models in which the fracture 18G01_2 was assigned a lower normal stiffness (models 2a (alt), 2b (alt)). Finally, the linear elastic near-field models focus on the changes in tangential stress for the different in situ stress conditions (model type 3, Fig. 4c and Fig. 6; models 3a, 3b, 3c, 3d).

For model type 2 including key fractures, focus in this paper is on presenting the results from in situ stress models *a* (strike-slip) and *b* (reverse, see Table 3).

5. Results and discussion

5.1. Large-scale models: influence of fracture zones

In order to assess the influence of the fracture zones (ID 04 and ID 10 & 12) on the stresses in the central parts of the TASO tunnel, i.e., the locations of the 300 mm holes, the large-scale models were analysed

Table 4
Models for the pore pressure in the fractures and fracture zones and for the internal pressure (swelling pressure from bentonite) in the 300 mm holes.

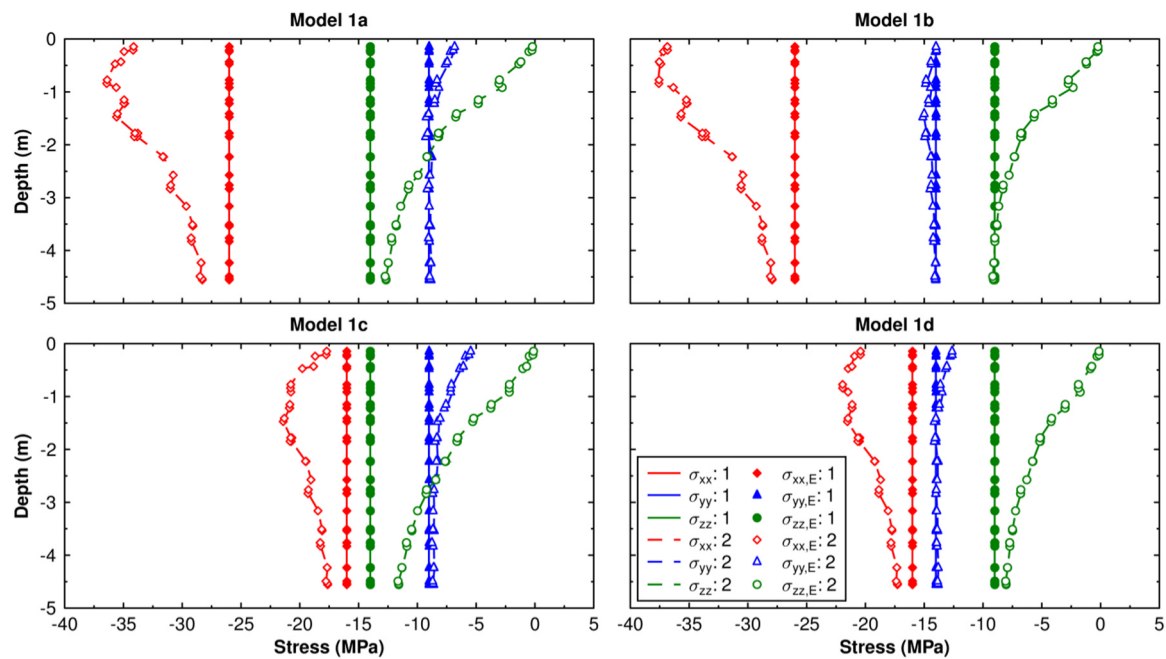| Modelling sequence	Discrete fractures (MPa)	Fracture zones (MPa)	Internal pressure (MPa)
1. Initial equilibrium (model types 1, 2, 3)	4	4	–
2. Excavation of tunnels (model types 1, 2, 3)	3	3	–
3. Pressurisation of fractures (model type 2)	1; 1.5; 2; 1.5; 1	–	–
4. Excavation of holes (model types 2, 3)	1	–	0
5. Swelling of bentonite (model types 2, 3)	1	–	0; 1; 2; 3

Fig. 8. Models (1a,c - strike-slip and 1b, d - reverse) – with active fracture zones (lines) or linear elastic (plot symbols). Stress components parallel to the model axes (σ_{xx}, across the tunnel; σ_{yy}, along the tunnel; σ_{zz}, vertical) at the midpoint between 17G01 and 18G01. "1": initial equilibrium and "2": state after excavation of tunnels. The same legend applies to all sub-figures.

either with these larger structures explicitly represented or without them (equivalent linear elastic models). Fig. 8 shows the stress components parallel to the model axes (σ_{xx}, across the tunnel; σ_{yy}, along the tunnel; σ_{zz}, vertical) at the midpoint between 17G01 and 18G01 as functions of depth below the tunnel floor. At these positions, the influence of the fracture zones is insignificant for all tested in situ stress models (Models 1a and 1c – strike slip, Models 1b and 1d – reverse; cf. Table 3). Therefore, boundary conditions for the smaller near-field models (types 2 and 3) were extracted from the linear elastic models.

5.2. Near-field models with fractures

The normal displacements, shear displacements and stability were evaluated at a number of points on each of the four fractures (see Fig. 9 for locations). Estimates of fracture stability are presented in terms of the Coulomb Failure Stress (*CFS*), which is evaluated as[17] $CFS = \tau - \sigma_n \tan\phi$, where τ is the shear stress, σ_N is the effective normal stress and ϕ is the friction angle. *CFS*-values that are less than zero represent stability. Displacements occurring during the initial equilibrium (modelling step 1) are not relevant for the purpose of this study and were, consequently, set to zero before excavation of the tunnels. The displacements presented in the figures below, therefore, represent changes relative to in situ conditions. Figs. 10–13 show the results for the fractures 17G01_1, 17G01_2, 18G01_1 and 18G01_2, respectively.

In Fig. 10 to Fig. 13, normal displacements are shown in the top row, shear displacements in the middle row and *CFS* in the bottom row. Results are presented for the selected history points on fractures, see Fig. 9, and as functions of modelling sequence (1 represents initial conditions, 2 excavation of the tunnels, TASO and TASD, 3a-e pressurisation of the fractures, see Table 4, 4 excavation of the 300 mm holes and 5a-c application of swelling pressure in the 300 mm holes, see Table 4). Each column represents a different assumption regarding the state of in situ stress. The presentation of results is focusing on Model a (strike-slip) and Model b (reverse), Table 3. The same legend applies to all sub-figures.

Based on these results, the normal displacements at the studied points on the four fractures were of the order of a few microns (opening

or closure) after excavation of the tunnels and during pressurisation of the fractures. After excavation of the 300 mm holes, the variations in normal displacements were larger with, in some cases, opening and closure occurring on different parts of the same fracture due to the heterogeneous stress-field around these holes.

Further, the assignment of a lower normal stiffness to fracture 18G01_2 (denoted 'alt' in the figures) appeared to have influenced only the magnitudes of the normal displacement of that fracture. Its influence on the response (normal or shear displacements) of the other fractures was minor. When considering the shear displacements, they were very small; the maximum recorded shear displacement at any of the points was of the order of 0.1 mm. In terms of fluid flow, the magnitude of the normal displacement influence the result. Assigning relevant values of normal stiffness is therefore of importance, particularly for the horizontal fracture close to the tunnel opening where radial stress can be expected to be lower, see further comments in Section 5.4.1.

Regardless of tested in situ stress model, the shear displacements appeared to have been mainly elastic. Some local inelastic deformations may have occurred during excavation of the 300 mm holes (see fractures 18G01_1 and 18G01_2 in model 2b, see Fig. 12 and Fig. 13 having a *CFS* of, or close to, zero). These inelastic deformations were in line with hydrogeological observations and measurements, see Section 5.4.2.

5.3. Linear elastic near-field models

The linear elastic near-field models aimed at assessing if e.g. the sub-vertical wetted trace observed in the bentonite parcel in 18G01 (Fig. 2, dashed line) could be initiated or opened after excavation of the 300 mm hole or after a swelling pressure of the bentonite had developed. The orientation of the sub-vertical structure had been determined to be 310°/90° (strike/dip), i.e., approximately perpendicular to the tunnel axis. Fig. 14 shows the horizontal stress component parallel to the tunnel axis (σ_{yy}), i.e., the tangential stress in the potentially most stress-relaxed part of the hole, as function of depth and modelling sequence. The modelling sequence (also in this case) include: 1 initial
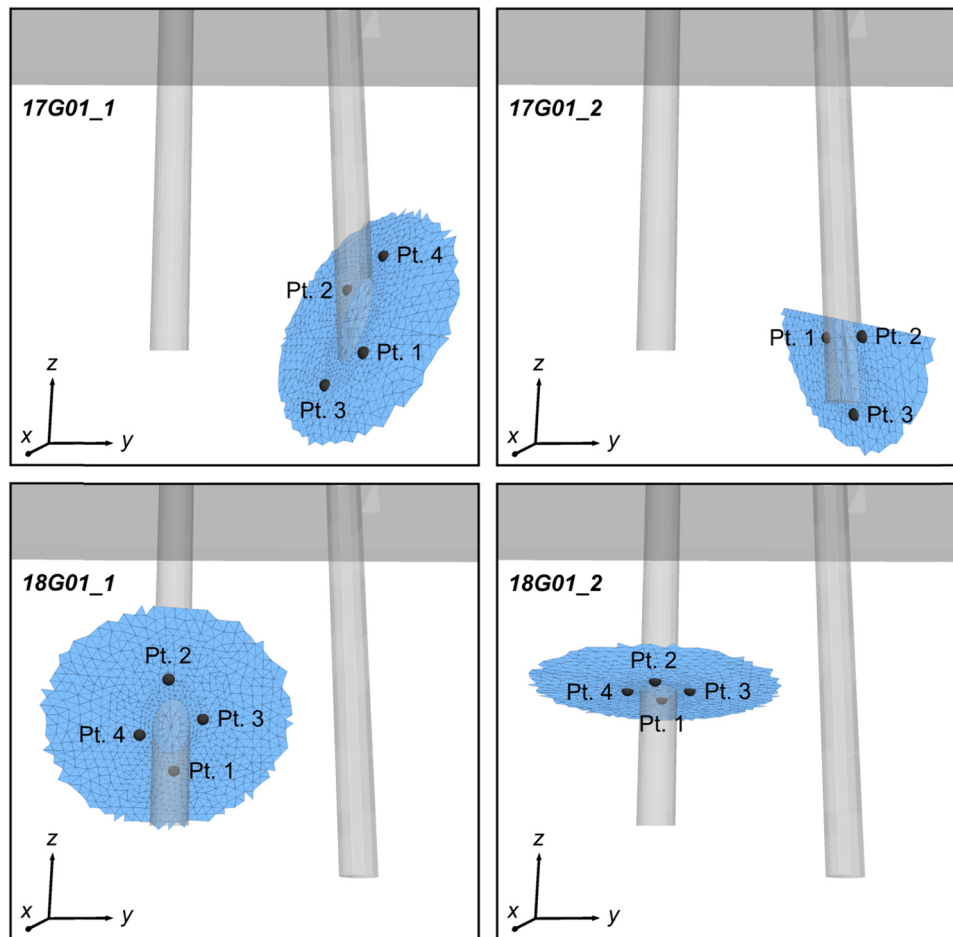
Fig. 9. Locations of history points on each fracture.

conditions; 2 excavation of the tunnels; 4 excavation of 18G01 and; 5a-c application of swelling pressures in the range 1–3 MPa. As before, each sub-figure represents a different assumption regarding the state of in situ stress (Table 3). Same legend applies to all sub-figures.

In model 3a (strike-slip), the stresses are tensile at all depths after excavation of 18G01. The application of a swelling pressure may increase the tensile stresses to values close to, or exceeding, the tensile strength of the rock in the uppermost parts of the hole. For the reverse type stress regime (model 3b), the stresses are compressive at all depths. The compression after excavation of the hole is, however, less than that during in situ conditions. This indicates a reduction in stress and a possible opening, in agreement with the orientation of vertical traces (models 3a to 3c), see Section 5.4.3.

In model 3c, the second strike-slip type stress regime (less difference between in situ stresses than model 3a), tensile stresses may develop in the uppermost parts of the hole. The magnitudes of the tensile stresses are less than the tensile strength. Finally, model 3d (the second reverse type stress regime), the stresses are compressive at all depths. The compression is greater than that during in situ conditions at all depths.

5.4. Field observations and measurements

Structural field mapping and characterisation, with specific focus on fracture geometry, kinematics, displacement and hydraulic properties, yielded results that appear to be in good agreement with the modelling results presented in Sections 5.1 to 5.3.

Key structural observations and measurements originated from the structural geological mapping of the TASO-tunnel and structural

logging of the recovered 300 mm cores in addition to hydrogeological characterisation of rock and bentonite parcels. These observations and measurements provided key inputs to the development of geometrical descriptions of the studied system and of its conceptualization and, in addition helped to validate geometrical and geomechanical assumptions implemented in the models.

5.4.1. Structural geological mapping

Section 4.3, Fig. 3 and Fig. 4 present the results of tunnel mapping and the model geometry that included two major fracture zones: ID 10 & 12 (representing clusters of several fractures) and ID 04. Based on structural geological mapping, ID 10 & 12 represents a distinct deformation zone that strikes NW-SE and contains fractures dipping steeply either to the NE or SW. The deformation zone is characterized by a higher fracture density in comparison to the less penetratively fractured wall rock. This permitted the definition of a clear, up to 200 mm thick damage zone for this fracture zone. Deformation zone ID 04 contains evidence of clear and sharp offset of a c. 30 cm thick granitic dyke within the host diorites that indicates a component of dextral shear along the fault zone.

The displacement was important both for the identification of this fracture as a full tunnel perimeter intersection and for the subsequent decision to include this fracture as an important feature in the model. A fracture that is identified as a full tunnel perimeter intersection has the potential to be a large and significant structural feature to the hydrogeological and mechanical behaviour of the system. Presence of damage zone and core as well as finite displacement can all be proxies for size of an investigated fracture.[18]
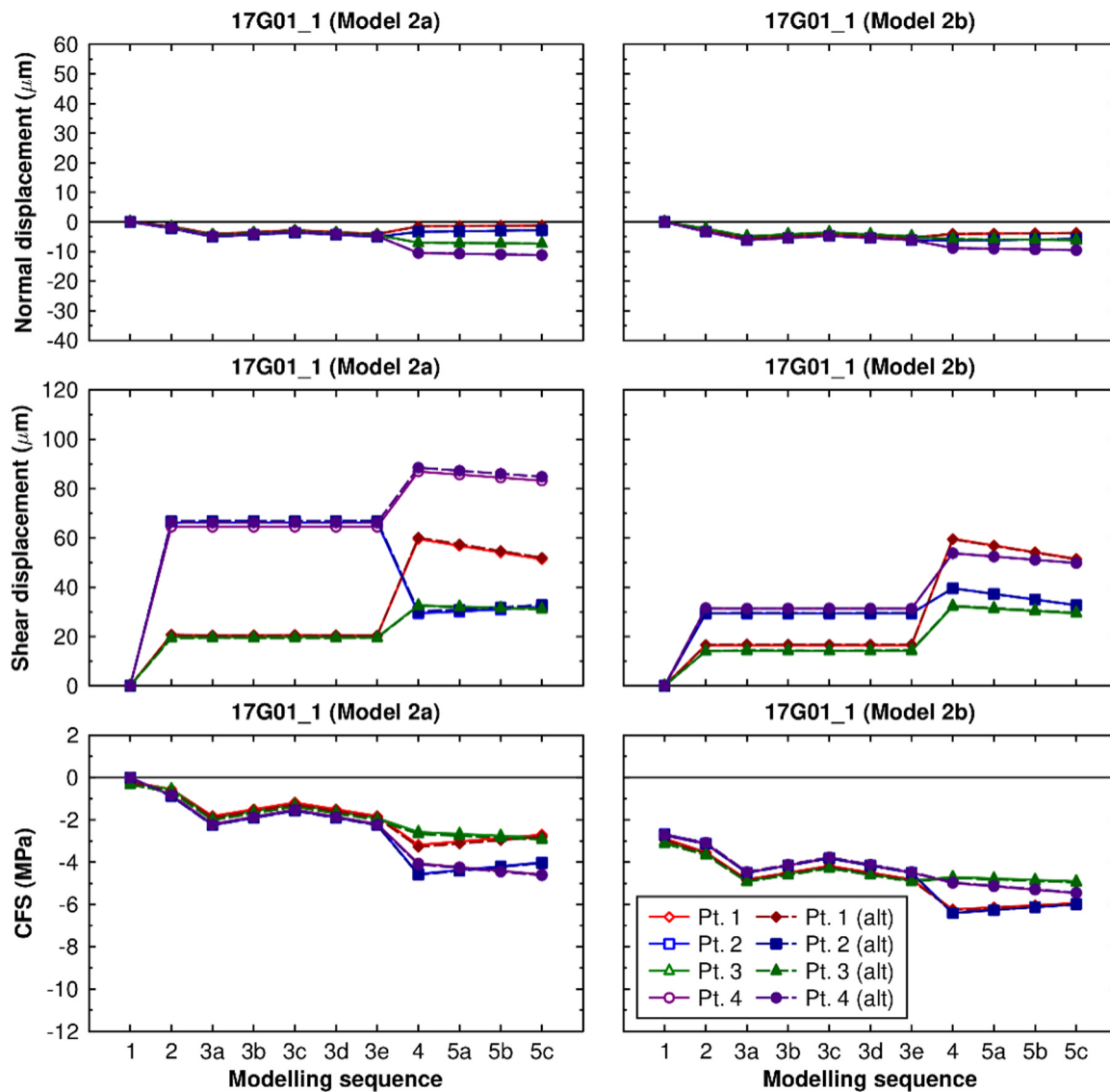
Fig. 10. Results from rock mechanical modelling (17G01_1 at history points, Fig. 9). Normal displacements (top row), shear displacements (middle row) and *CFS* (bottom row) as functions of modelling sequence (1–5c). Two states of in situ stress (Model 2a – strike-slip, Model 2b – reverse).

Using field data, fractures and deformation zones at the site were sorted into five systematic sets on the basis of the orientation and geometry. The two major fracture zones mentioned above, in addition to the fracture identified along the pegmatite vein in 17G01 (17G01_2, see Table 1) and the main fracture in borehole 17G01, 17G01_1 belong to a fracture set striking perpendicular to the tunnel (strike WNW- to NW, or NW-SE) and are moderately to steeply dipping either to the NE or SW. The main fracture of interest in 18G01 (18G01_1) belongs to a second fracture set that is subparallel to the tunnel with strike ENE-WSW and has a moderate dip to NW. The second distinct fracture in 18G01 (18G01_2), as well as a subhorizontal ductile precursor shear zone belongs to a third set that consists of moderately to gently dipping fractures (18G01_2 strikes SW-NE and dips at very low angle to the NW). In addition to these three sets we could define a systematic set of subvertical to very steep SSW-SW fractures and a set of subvertical E-W fractures.

Focus for the integrated investigation has been borehole 18G01 due to the hydraulic changes observed in this borehole. Considering fracture mechanical properties, the structural mapping indicated localized to the SE reverse faulting, as constrained by striations in 18G01_1 (part of the fracture set subparallel to the tunnel). Structural characterisation

thus indicated a planar anisotropy that may lower resistance to deformation.

The mechanical properties of single fractures that were used for the mechanical modelling[13], see Table 2, were based on two types of previously performed laboratory tests: direct shear- and normal stiffness tests on small fracture-containing samples and the so called tilt tests, also using small fracture-containing samples from the drill cores. Mean peak friction angle for tested samples was 37° with a standard variation of 3.2°. Mean peak cohesion 0.9 MPa. Normal stiffness had a large min-max span of 70–4000 GPa/m.

Suggesting that the selection of individual fracture properties (including fracture surface anisotropy) for modelling can be more specific and related to fractures and fracture sets, it would be reasonable to select/consider lower (range) values of shear stiffness and friction angle due to the planar anisotropy identified for e.g. 18G01_1.

Low (radial) stress below the tunnel floor due to excavation may also allow a lower (range) value of normal stiffness (represented in the mechanical modelling using 700 GPa/m or 70 GPa/m, see Table 2). A lower value resulting in an increased normal displacement. Previously performed on site investigations of deformation based on hydraulic testing (change in estimated hydraulic aperture) and direct deformation
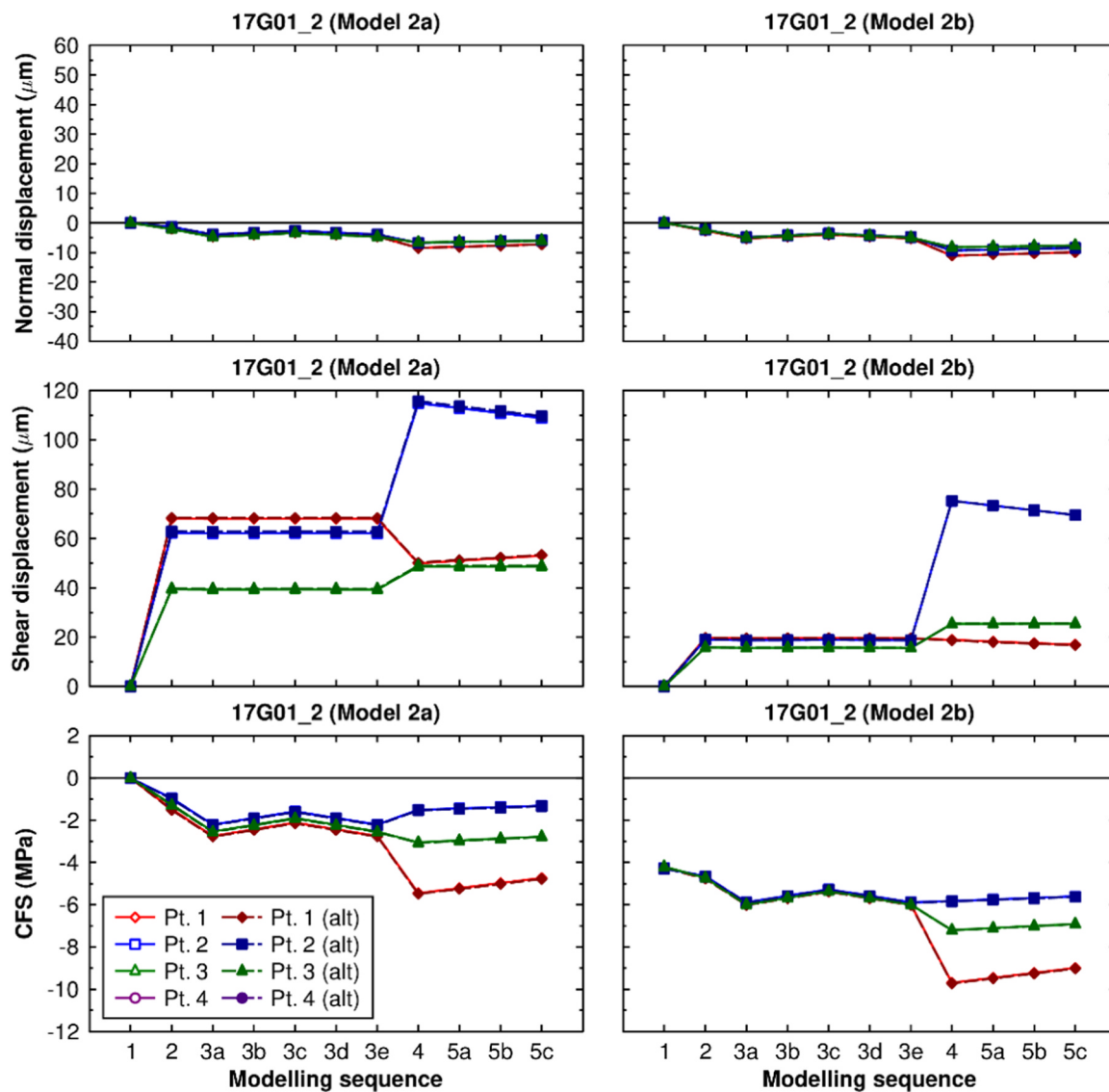
Fig. 11. Results from rock mechanical modelling (17G01_2 at history points, Fig. 9). Normal displacements (top row), shear displacements (middle row) and *CFS* (bottom row) as functions of modelling sequence (1–5c). Two states of in situ stress (Model 2a – strike-slip, Model 2b – reverse).

measurements presented low range values of stiffness (below 100 GPa/m), thus suggesting a low stiffness for investigated fractures below the floor and close to the tunnel opening.[16,19]

Besides providing information about the key fractures in the model, the structural mapping allowed to establish solid relationships between brittle structural features in the tunnel and in the cores, which were used as or compared to the main fracture input to the rock mechanical modelling. These fracture sets are also structurally reconcilable with the larger-scale tectonic picture of the area.[7]

The above suggests that with an integrated approach, the selection of individual fracture properties (including fracture surface anisotropy) for modelling can be more specific and more appropriate to reproduce the natural conditions as indicated by detailed, deterministic structural mapping.

5.4.2. Hydrogeological characterisation of rock and bentonite parcels

Mechanical modelling presents displacements (small but still). Observations and measurements at the site did initially show "no" (very low) flow for the lower part of the 76 mm borehole 18G01. The lower part of the borehole was therefore considered to be dry. During hydraulic characterisation of the overcored borehole (300 mm diameter,

depth 2.1–3.1 m) a flow of 0.01–0.02 ml/min was measured. A rough estimate of an hydraulic aperture assuming a parallel plate model, using the cubic law (Snow, 1968) and suggesting that transmissivity is approximately equal to the specific capacity results in an aperture of a few μm, ($Q/dh \approx T = \rho g b^3/12\,\mu$, Q: 0.01 ml/min and dh: 100 m). This (change in) hydraulic aperture would be in the same order of magnitude as the modelled normal displacement (a few μm), see fractures 18G01_1 and 18G01_2, Model 2b, upper row, in Fig. 12 and Fig. 13.

For fractures 18G01_1 and 18G01_2, wet traces on bentonite confirmed that the steep fractures were water-bearing and water content plots show significant wetting in the upper (and less clearly in the lower) part of their traces. This is in line with the modelling results were local inelastic deformations may have occurred during excavation of the 300 mm holes (see fractures 18G01_1 and 18G01_2, model 2b, Fig. 12 and Fig. 13. Modelling results, e.g. fracture 18G01_1 (Model 2b, a reverse stress regime, σ_H: −26 MPa; σ_h: −14 MPa; σ_v: −9 MPa, see Fig. 12) would be in agreement with the deep wetting indicated at the upper part of fracture 18G01_1 (Pt. 2) where the Coulomb Failure stress, *CFS* (presented in the lower row Fig. 12) goes to zero. This points at an agreement between the spatial locations of changes in flow identified from the bentonite parcels and the locations of inelastic
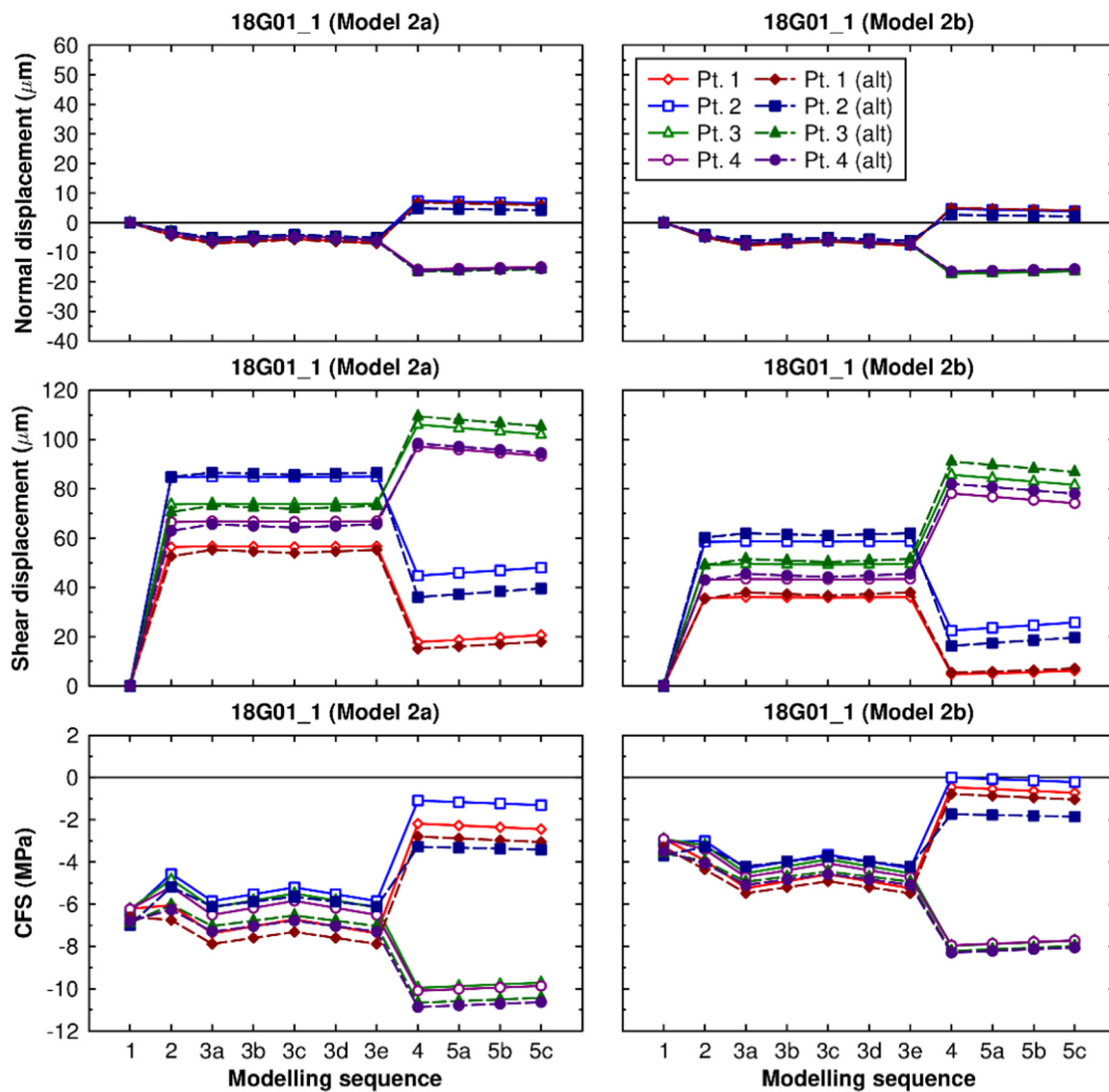
Fig. 12. Results from rock mechanical modelling (18G01_1 at history points, Fig. 9). Normal displacements (top row), shear displacements (middle row) and *CFS* (bottom row) as functions of modelling sequence (1–5c). Two states of in situ stress (Model 2a – strike-slip, Model 2b – reverse).

deformation indicated by mechanical modelling for a reverse stress regime.

5.4.3. Vertical traces on bentonite

Significant wetting for both 17G01 and 18G01 was also demonstrated by a few traces running subparallel to the drill core axis (see e.g. dashed line next to wetted trace in Fig. 2). This was investigated using a linear elastic near-field model, see Section 5.3.

For 17G01 flow corresponding to the wetting seen at the modelled orientation was identified neither in the 300 mm borehole, as imaged by photographs of the borehole wall, nor by a "nappy" test[1] whereby the flow was measured directly inside the borehole by using sorbing material laid directly against the borehole wall.

Rock mechanical modelling shows successive reductions of the tangential stress for the 300 mm tunnel floor borehole at positions perpendicular to the tunnel axis. This is a possible explanation for the wetting in 17G01 along the pegmatite vein but could not explain the wetting along e.g. 18G01 in sections where no fractures were identified on the borehole cores.

6. Concluding remarks

For all four tested in situ stress models, the two modelled fracture zones ID 04 and ID 10 & 12 were stable during initial conditions. Any subsequent displacements of the fracture zones induced by the excavation of the tunnel did not appear to influence the state of stress in the rock surrounding 17G01 and 18G01. The fracture zones were, therefore, not considered in the near-field models and boundary conditions for these models were obtained from linear elastic versions of the large-scale models.

The normal displacements at the studied points on the four selected fractures were of the order of a few microns (opening or closure) after excavation of the tunnels and during pressurisation of the fractures. After excavation of the 300 mm holes, the variations in modelled normal displacements were larger with, in some cases, opening and closure occurring on different parts of the same fracture. The assignment of a lower normal stiffness to the sub-horizontal fracture (18G01_2) appears to have influenced the magnitudes of the normal displacement of that fracture, while the influence on the response (normal or shear displacements) of the other fractures was minor. Based on the results, modelled and estimated changes in (hydraulic) aperture
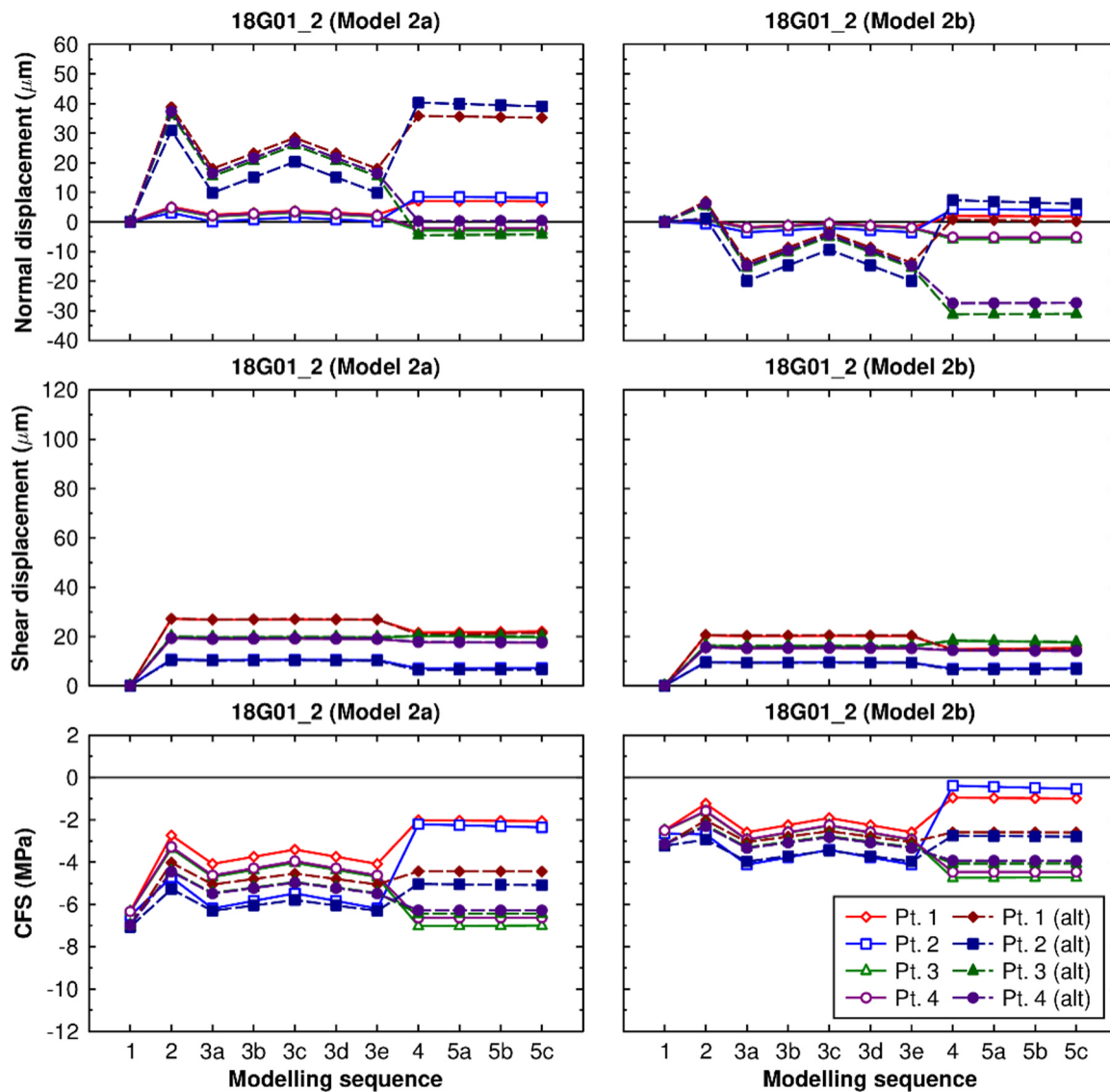
Fig. 13. Results from rock mechanical modelling (18G01_2 at history points, Fig. 9). Normal displacements (top row), shear displacements (middle row) and *CFS* (bottom row) as functions of modelling sequence (1–5c). Two states of in situ stress (Model 2a – strike-slip, Model 2b – reverse).

(using field observations) were in the same order of magnitude (a few µm).

Shear displacements at the studied points on the four fractures were small (order of at most 0.1 mm) and appeared to be mainly elastic. Location of inelastic deformation (e.g. upper part of borehole-fracture intersection, Pt. 2, in 18G01_1) was in agreement with the location of observed and measured deep wetting on bentonite.

Based on the above a reverse stress regime results in consistency between mechanical deformation and the borehole flow observations for BRIE.

Reductions in the tangential stress at positions perpendicular to the tunnel axis were obtained in three out of the four analysed linear elastic near-field models, thus indicating potential for opening of pre-existing sub-vertical fractures striking perpendicular to the tunnel and intersecting 18G01 in the most stress-relaxed parts of the hole. Sub-vertical traces with deep wetting were also identified on bentonite perpendicular to the tunnel axis (same orientation). Opening of existing fractures (e.g. fracture 17G01_2 along the vein) is a valid explanation but for the generation of new fractures, further investigating and modelling

the brittle behaviour of rock locally at the borehole wall would be of interest.

As summarized above, modelled fracture normal- and shear displacements were found to be local, small and in line with field observations and measurements for BRIE. Besides providing information about the key fractures in the model, the structural mapping allowed to establish solid relationships between brittle structural features in the tunnel and in the cores, which were used as or compared to the main fracture input to the rock mechanical modelling. The identified fracture sets were found to be structurally reconcilable with the larger-scale tectonic picture of the area. Based on the results from the site, we conclude that step-wise rock mechanical modelling, integrated structural mapping and hydrogeological investigations can indeed bring additional value to a full rock description and to the understanding of the hydromechanical behaviour of a rock volume. Semiquantitative agreement between the performed investigations is relevant and gives additional (independent) constraints to parameters and system behaviour.
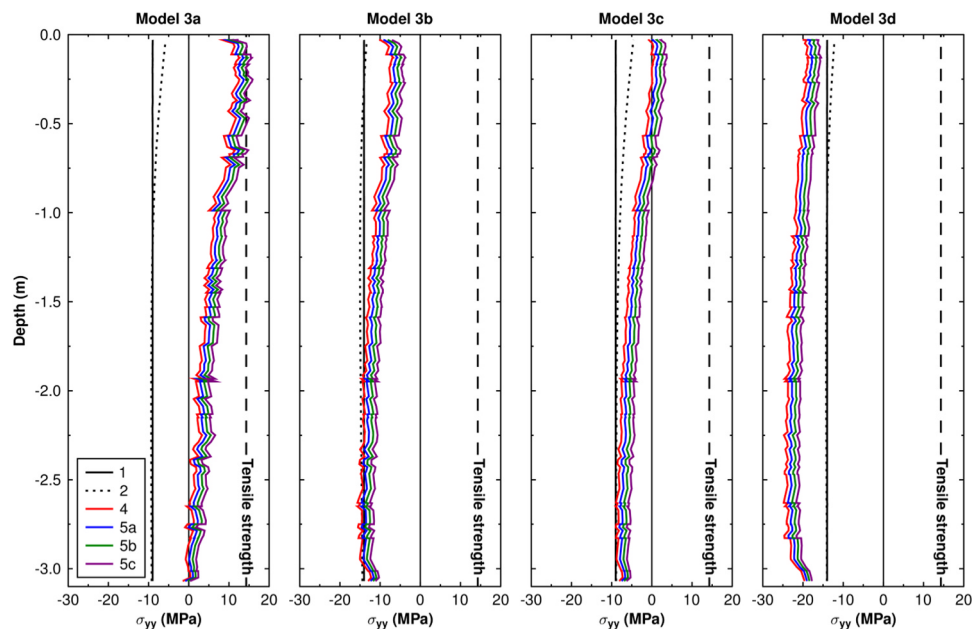
Fig. 14. Stress (stress regimes a-d) for vertical traces/structures (perpendicular to tunnel axis, see orientation of wetted trace indicated by dashed line in Fig. 2). Tangential stress, in the potentially most stress-relaxed part of the hole, as function of depth and modelling sequence.

Acknowledgements

References

1. Fransson Å, Åkesson M, Andersson L. *Bentonite Rock Interaction Experiment Characterization of rock and installation, hydration and dismantling of bentonite parcels. SKB report R-14-11.* Stockholm, Sweden: Swedish Nuclear Fuel and Waste Management Co; 2017.
2. SKB. *Long-term safety for the final repository for spent nuclear fuel at Forsmark. Main report of the SR-Site project. SKB report TR-11-01.* Stockholm, Sweden: Swedish Nuclear Fuel and Waste Management Co; 2011.
3. Dessirier B, Frampton A, Fransson Å, Jarsjö J. Modeling early in situ wetting of a compacted bentonite buffer installed in low permeable crystalline bedrock. *Water Resourc Res.* 2016;52:6207–6221.
4. Dessirier B, Åkesson M, Lanyon B, Frampton A, Jarsjö J. Reconstruction of the water content at an interface between compacted bentonite blocks and fractured crystalline bedrock. *Appl Clay Sci.* 2017;142:145–152.
5. Holton D, Baxter S, Hoch AR. Modelling coupled processes in bentonite: recent results from the uk's contribution to the Äspö EBS Task Force. *Mineral Mag.* 2012;76:3033–3043.
6. Hancilova I, Hokr M. Coupled hydro-mechanical model of bentonite hydration and swelling. *IOP Conf Ser: Earth Environ Sci.* 2016;44:032024.
7. Viola G, Venvik Ganerod G, Wahlgren C-H. Unraveling 1.5 Ga of brittle deformation history in the Laxemar-Simpevarp area, southeast Sweden: a contribution to the Swedish site investigation study for the disposal of highly radioactive nuclear waste. *Tectonics.* 2009;28:TC5007.
8. Itasca. 3DEC 5.0 – 3-Dimensional Distinct Element Code. User's Guide. Itasca Consulting Group, Inc., Minneapolis, Minnesota; 2013.
9. Lemos J. Block modelling of rock masses: concepts and application to dam foundations. *Eur J Environ Civil Eng.* 2008;12:915–949.
10. Lönnqvist M, Hökmark H. *Thermal and thermo-mechanical evolution of the Äspö Prototype Repository rock mass. Modelling and assessment of sensors data undertaken in connection with the dismantling of the outer section. SKB report R-13-10.* Stockholm, Sweden: Swedish Nuclear Fuel and Waste Management Company; 2015.
11. Brady BHG, Brown ET. *Rock Mechanics for Underground Mining.* 2nd ed. London: Chapman & Hall; 1993.
12. Staub I, Andersson JC, Magnor B. *Äspö pillar stability experiment. Geology and mechanical properties of the rock in TASQ. SKB report R-04-01.* Stockholm, Sweden: Swedish Nuclear Fuel and Waste Management Co; 2004.
13. Hakami E, Fredriksson A, Lanaro F, Wrafter J. *Rock mechanics Laxemar. Site descriptive modelling. SDM-Site Laxemar. SKB report R-08-57.* Stockholm, Sweden: Swedish Nuclear Fuel and Waste Management Co; 2008.
14. Lönnqvist M, Hökmark H. Assessment of method to model slip of isolated, non-planar fractures using 3DEC. In: *Proceedings of the 13th International Symposium on Rock Mechanics,* Montreal. ID 2015-2265; 10-13 May 2015.
15. Janson T, Stigsson M. *Test with different stress measurement methods in two orthogonal bore holes in Äspö HRL. SKB report R-02-26.* Stockholm, Sweden: Swedish Nuclear Fuel and Waste Management Co; 2002.
16. Thörn J. *Hydromechanical Behaviour of Fractures Close to Tunnels in Crystalline Rock [Licentiate thesis].* Göteborg, Sweden: Chalmers University of Technology; 2013.
17. Harris RA. Introduction to special section: stress triggers, stress shadows, and implications for seismic hazard. *J Geophys Res: Solid Earth.* 1998;103(B10):24347–24358.
18. Cosgrove J, Stanfors R, Röshoff K. *Geological characteristics of deformation zones and a strategy for their detection in a repository. SKB report R-06-39.* Stockholm, Sweden: Swedish Nuclear Fuel and Waste Management Co; 2006.
19. Thörn J, Fransson Å. Assigning fracture stiffness from in-situ deformation measurement. In: *Proceedings of the 1st International Discrete Fracture Network Engineering Conference.* Vancouver ID 2014-2171; 20–22 October 2014.